PHYSICAL REVIEW A, VOLUME 62, 023403

Nonsequential double ionization of small molecules induced by a femtosecond laser field

C. Cornaggia and Ph. Hering
CEA Saclay, Direction des Sciences de la Matière, Service des Photons, Atomes et Molécules,
Bâtiment 522, F-91 191 Gif-Sur-Yvette, France

(Received 9 August 1999; revised manuscript received 15 March 2000; published 17 July 2000)

Nonsequential double ionization of several molecules such as N_2, CO_2, C_2H_2, and C_3H_4 in strong laser fields has been unambiguously identified from the ion-yield measurements in comparison with a sequential ionization model in the $10^{13}-10^{15}$ W/cm^2 laser intensity range. This effect is observed mainly using linearly polarized laser light. In circular polarization, nonsequential double ionization might be present, for instance for the C_2H_2 molecule, but with a much lower contribution than in linear polarization. The experimental method allows us to detect all the double-ionization decay channels that are the molecular dication and the two-missing electron fragmentation channels. The validity of a single-ionization tunneling model developed for atoms has been extended to molecules, and a good agreement is observed in laser intensity ranges where single-ionization processes take place.

PACS number(s): 33.80.Rv, 33.80.Eh

I. INTRODUCTION

Laser-induced nonsequential multiple ionization has been studied in more details in atoms [1,2] than in molecules. To our knowledge, the first reports on nonsequential double ionization of molecules appeared in 1997 with the work of Talebpour *et al.* on the NO molecule [3] and in 1998 with the work of our group [4]. This paper is intended to present a complete set of experimental data recorded with different molecules such as N_2, CO_2, C_2H_2, and C_3H_4 and an improved interpretation of molecular ionization using intense femtosecond laser pulses. The choice of these diatomic and polyatomic molecular species among all the molecules studied in our laboratory is intended to show that laser-induced nonsequential double ionization is a common feature in atomic and molecular physics.

The simplest way to understand the multiple ionization of atoms and molecules is to assume that electrons are removed in a sequential way, since the energy of the laser photon is much smaller than the different ionization potentials. For the single ionization of neutral atoms, a lot of models have been proposed in the past. If the number of absorbed photons exceeds 4 or 5, the multiphoton approach is difficult to deal with because the transition amplitude calculations involve the summation over an increasing number of intermediate states [5]. Alternative approaches based on tunnel ionization have been proposed in the 1960s with the advent of laser beams able to ionize atoms [6,7]. These methods have been adapted to complex atoms [8,9] while, at the same time, the numerical integration of the Schrödinger equation becomes possible in the nonperturbative regime due to the progresses of the computation facilities [10]. These different approaches involve a single active electron and were compared with success to the experimental data for the ionization of neutral atoms [10,11]. The same methods were applied to the sequential ionization of atoms: the single-ionization rates are calculated for the neutral, singly charged ion, and so on. However, the measured double-ionization yields were found to be orders of magnitude higher than the theoretical predictions in the case of helium [1,12,10], neon, argon, and xenon [13] at low laser intensities. Recently, the experimental studies were extended to ions with charge states higher than 2, with the same conclusions about the failure of the sequential models [13]. It is concluded that nonsequential electron emission processes play a significant role in high laser fields. Theoretical efforts are underway to involve more than one active electron in the calculations, in particular to interpret the double-ionization ion yields measured with rare-gas atoms [2,14,15]. Finally let us mention the early models proposed by experimentalists to explain nonsequential double ionization. Fittinghof *et al.* proposed a shake-off process [12]: the escape of the outer electron produces a rapid change in the potential experienced by the inner electron and as a consequence an enhancement of the ionization rate. On the other hand, Corkum proposed a different mechanism based on electron-electron inelastic rescattering [16]. The outer electron is ejected from the neutral atom and oscillates in the strong laser field. This electron can revisit the core after at least a half-laser period and knock off the inner electron.

Single ionization of neutral molecules by intense femtosecond laser pulses remains an active area of research since the atomic models have to be adapted to the molecular field [17]. Several methods were proposed to improve the agreement with the experimental data for light molecules such as D_2 [18], unsaturated hydrocarbons [19], or heavier molecules [20]. Concerning the nonsequential double ionization, theoretical efforts are underway following the first trials with atoms [21]. To our knowledge, experimental investigations do not give the same wealth of results as in the atomic case.

The study of double ionization presented in this paper is based on the measurements of the cation and dication yields as a function of the laser intensity at $\lambda = 800$ nm in the $10^{13}-5\times10^{15}$ W/cm^2 laser intensity range using a 50-fs laser-pulse duration. The experimental results are compared with a kinetic model where single-ionization rates of the neutral and single charged molecules are introduced in the equations. The molecular single-ionization rates are calculated following the tunneling theory developed by Perelomov *et al.* for atoms [7], with some modifications in order to take into account the molecular electronic wave function of the escaping electron. Consequently, the kinetic model is valid only for a sequential electron ejection to reach the double-ionization thresholds. The observed deviations between the experimental measurements and the model predictions are interpreted by the presence of nonsequential double-ionization processes. In addition, the experiments and calculations are performed in linear and circular polarizations, since the atomic nonsequential double ionization has been observed using only linearly polarized laser light. Indeed the rescattering model introduced by Corkum was successful in interpreting the absence of nonsequential processes in circular polarization, since in this case the first ejected electron does not return to the vicinity of the ionic core [16].

Molecular dications are metastable since their fundamental electronic state is dominated by the Coulomb repulsion of their constituents at large internuclear distances. At short internuclear distances, they exhibit a bonding structure due to covalent forces. The double-ionization decay channels are molecular dications and fragmentation channels involving two singly charged fragments. The weak contribution of fragmentation channels involving a neutral fragment and a doubly charged fragment is not taken into account [4]. In the present study, the fragmentation channels are identified using the covariance mapping technique [22]. In Ref. [4] we showed that for N_2 the observed decay channels ${N_2}^{2+}$ and $N^+ + N^+$ come from the same complex $[{N_2}^{2+} + 2e^-]$ following the laser excitation. Similar results are obtained for the ${CO_2}^{2+}$ and $O^+ + CO^+$ decay channels of CO_2. Consequently, it is possible to sum the ion yields from these decay channels to get the overall ion yield from the double-ionization process. However, for molecules such as C_2H_2 and C_3H_4, the situation is more complex due to the presence of several bonds, and only the detected molecular dication yields are reported here and compared with the sequential calculation. Indeed in C_2H_2, the two-missing electron fragmentation channels are very weak, while in C_3H_4 a more detailed discussion will be presented in Sec. IV, which presents the experimental results. Finally the molecular multiple ionization, involving more than two removed electrons, is not taken into account in this paper because below the laser saturation intensities for the single and double ionization of molecules, the corresponding ion yields remain very low in comparison with the singly and doubly charged molecular ion yields. Above the laser saturation intensity, the multiple ionization might in some cases reduce the cation and dication signals, but with a minor contribution due to the short pulse duration used in these experiments. This point will be commented on in Sec. IV for the CO_2 case.

II. EXPERIMENTAL SETUP

A. Laser system and beam profile

The laser system is a femtosecond kilohertz laser chain built around the *titanium-sapphire* laser gain medium technology. A self-mode locked oscillator delivers 27-fs laser pulses with a wavelength spectrum centered at $\lambda = 800$ nm. The amplification is based on the chirp-pulse amplification technique [23]: the input laser pulses are stretched to a duration $\tau = 300$ ps before their injection in the regenerative amplifier pumped by a kilohertz Nd^{3+}:YLF laser. The pulses are extracted from the amplifier at the recurrence of 1 kHz and recompressed to $\tau = 40$ fs using a two-grating compressor. The laser pulse durations are measured using standard second-order autocorrelation techniques [24]. The laser-pulses energy is typically 700μJ at $\tau = 40$ fs and $\lambda = 800$ nm.

The laser beam is focused in the high vacuum chamber using a fused silica spheroparabolic lens corrected for spherical aberrations. Systematic measurements of the pulse duration were done at the exit window of the experimental chamber in order to investigate the pulse-duration broadening due to group velocity dispersion (GVD). An upper limit of the pulse duration inside the vacuum chamber is $\tau = 50 \pm 5$ fs in this case, using the compressor to compensate the GVD in the fused silica entrance window and lens. The beam profile has been measured and in particular the M^2 factor which characterizes the difference of the effective laser beam with an ideal Gaussian laser beam [25]. In brief, the laser intensity $I(r,z)$ of a Gaussian beam is [26]

$$I(r,z) = I_0 \left[\frac{w(0)}{w(z)}\right]^2 \exp\left\{-2\left[\frac{r}{w(z)}\right]^2\right\}, \tag{1}$$

where the z axis represents the direction of propagation. For an ideal Gaussian beam, the radius at $1/e^2$ in the z plane is given by $w^2(z) = w_0^2[1 + (z/z_0)^2]$, where w_0 is the radius at $I(r = w_0, z = 0) = I_0/e^2$ and $z_0 = \pi w_0^2/\lambda$ is the Rayleigh range. The M^2 parameter appears in the propagation of a real laser beam as $w^2(z) = w_0^2[1 + (M^2 z/z_0)^2]$ [25]. This parameter has been measured for our laser, $M^2 = 1.77$, and the spot area is $\pi w_0^2 = 2.8 \times 10^{-6}$ cm^2. The ion yields are measured as a function of the peak laser intensity represented by I_0 in Eq. (1).

Finally, the laser energy is varied using a zero-order half-wave plate and two reflecting polarizers. The output laser beam energy is calibrated as a function of the angle of the half-wave plate with the initial polarization direction. In the case of experiments performed with circular polarization, an additional zero-order quarter-wave plate is put after the polarizers system.

B. Ion-yields measurements

The atomic and molecular ions are identified using a time-of-flight mass spectrometer equipped with high transparency grids and a 40-mm effective diameter microchannel plate detector. The short drift tube (100 mm) and the effective Rayleigh range $z_M = z_0/M^2 = 200$ μm ensure that all the ions produced in the interaction volume are detected. The absolute numbers of ions are determined from the overall ion transmission of the spectrometer, the detection efficiency, and the gain of the microchannel plate (MCP) detector. The ion spectrometer is equipped with three $T = 90\%$ high transparency grids that give a $T^3 = 73\%$ total ion transmission. The MCP detector efficiency is given from the GALILEO company data worksheets and is estimated to be $\eta_d = 50\%$ for 2.5 keV impinging ions. This number is not too far from the open area ratio of the detector, which is 63% and pre-

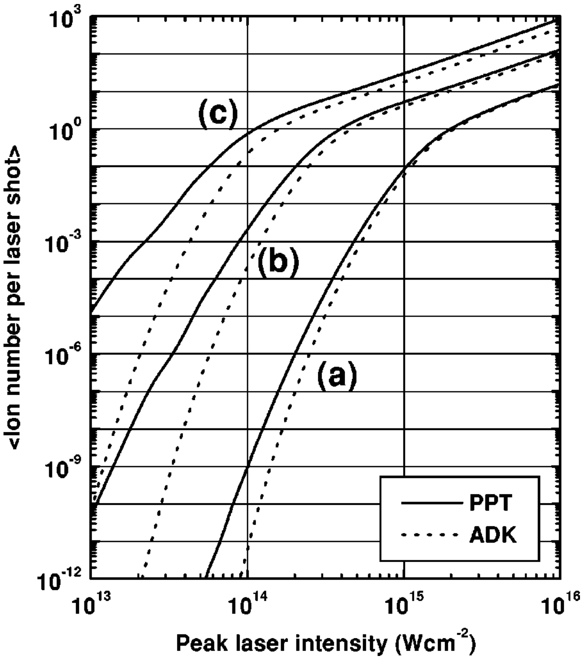

FIG. 1. Calculated singly charged ion number per laser shot for a reference pressure $p = 10^{-9}$ Torr as a function of the peak laser intensity for linearly polarized laser light using the (—) PPT and (···) ADK ionization rates for (a) helium, (b) molecular nitrogen, and (c) acetylene.

sents an accuracy of ±20%. As a consequence, the overall ion detection efficiency is $\eta = T^3 \eta_d = 36\%$. Finally, the average detector gain is calibrated from single–ion signals.

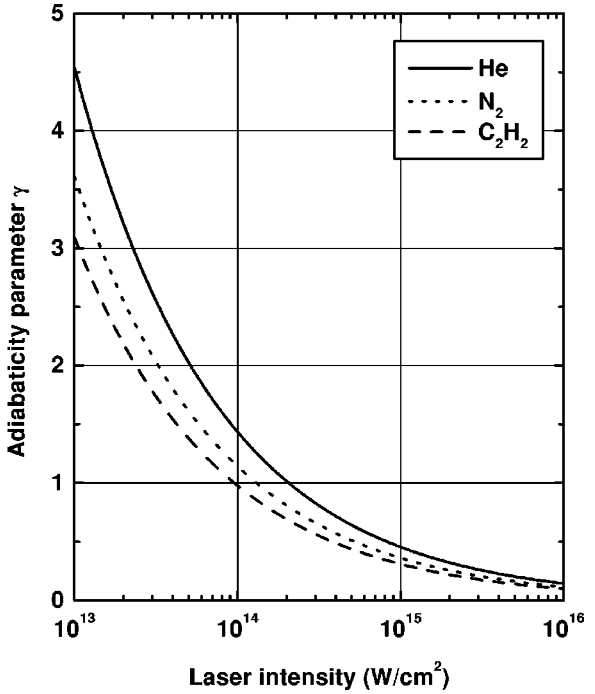

FIG. 2. Adiabaticity parameter γ as a function of the laser intensity for (—) helium, (···) molecular nitrogen, and (– –) acetylene. The laser polarization is linear.

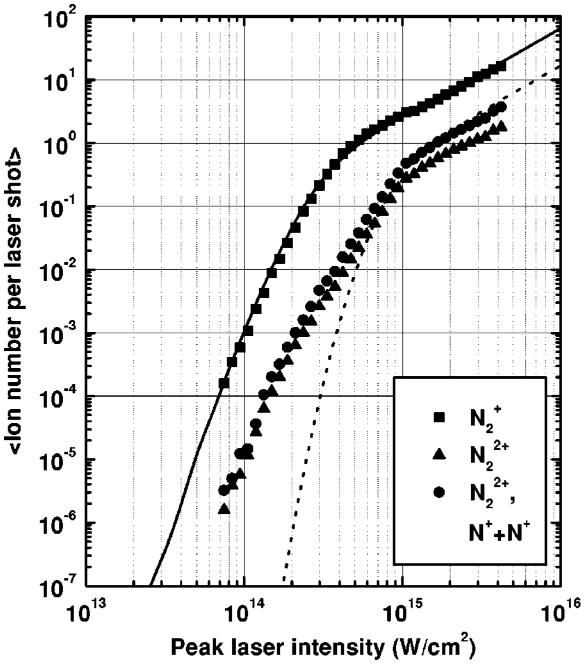

FIG. 3. Experimental (squares, N_2^+; up triangles, N_2^{2+}; and circles, $N^+ + N^+, N_2^{2+}$) and calculated average ion numbers per laser shot for a reference pressure $p(N_2) = 10^{-9}$ Torr as a function of the peak laser intensity for linearly polarized laser light. The model predictions are represented by the full curve (—) for single ionization and the dotted curve (···) for sequential double ionization. The experimental total contribution of double ionization is represented by the sum (●) of the detected N_2^{2+} dications and N^+ ions from the $N^+ + N^+ + E_{\text{Kinetic}}$ channels with 5.6 eV$\leqslant E_{\text{Kinetic}} \leqslant$11.6 eV.

In these experiments it is important to detect only a few ions so that the detector response remains linear as a function of the number of impinging ions. The gas pressure is adjusted in order to detect no more than 10 ions per laser shot and is varied from 10^{-9} Torr in the 10^{15} W/cm^2 laser intensity range to 10^{-5} Torr in the 10^{13} W/cm^2 intensity range. For each laser intensity, the ion signal is averaged over more than 20 000 laser shots in order to get rid of the detector fluctuations. The ion yields in Figs. 1–7 are presented for a reference pressure of 10^{-9} Torr. This pressure is the real gas pressure inside the vacuum chamber, and takes into account the corrective factors of the ionization gauge applied for each gas species.

The ion-ion fragmentation channels are identified using the covariance mapping technique [22], and an example is given in our previous paper for the $N^+ + N^+$ fragmentation channel with the associated kinetic-energy release spectrum [4]. Moreover, this technique is used extensively in our laboratory for the overall fragmentation identification of molecules in strong laser fields, and consequently is not described in this paper [27]. Concerning the different fragmentation channels, the $N^{2+} + N + 2$ eV channel is also detected in the experiments. Indeed the presence in the time-of-flight spectra of N^{2+} ions that are not correlated to any other ion signals is the signature of the existence of this dissociation pathway. However, this channel branching ratio is very weak in comparison with the $N^+ + N^+$ branching ratio because the $N^{2+} + N$ fragmentation threshold $E(N^{2+}$

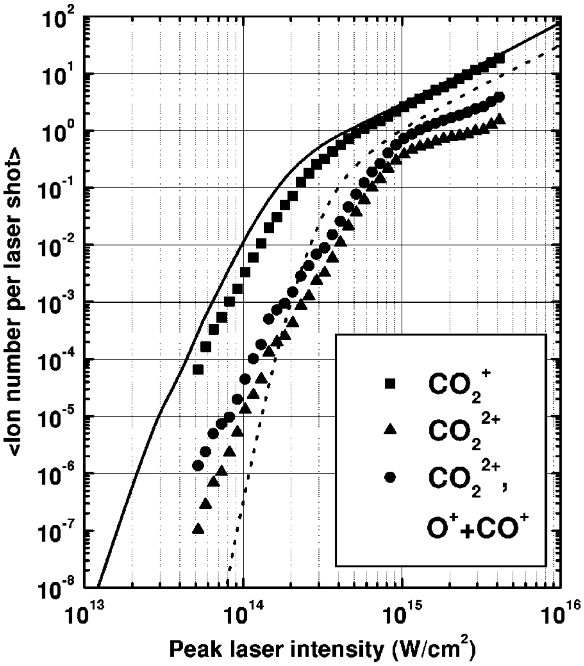

FIG. 4. Experimental (squares, CO_2^+; up triangles: CO_2^{2+}; and circles, $O^+ + CO^+, CO_2^{2+}$) and calculated average ion numbers per laser shot for a reference pressure $p(CO_2) = 10^{-9}$ Torr as a function of the peak laser intensity for linearly polarized laser light. The model predictions are represented by the full curve (—) for single ionization and the dotted curve ($\cdots$) for sequential double ionization. The experimental total contribution of double ionization is represented by by the sum (●) of the detected CO_2^{2+} dications and O^+ ions from the $O^+ + CO^+ + E_{\text{Kinetic}}$ channels with 3.6 eV $\leqslant E_{\text{Kinetic}} \leqslant 6.8$ eV.

$+N$) is higher than the $N^+ + N^+$ fragmentation threshold $E(N^+ + N^+)$ following $E(N^{2+} + N) - E(N^+ + N^+) = 15.07$ eV.

III. SEQUENTIAL IONIZATION IN STRONG LASER FIELDS

A. Atomic single-ionization rates

The photon energy at $\lambda = 800$ nm is $E_p = 1.55$ eV and 11 and 18 photons are at least necessary to ionize, respectively, N_2 and N_2^+. As a consequence, the lowest-order perturbation theory is unpractical for the computation of ionization rates. In addition, this approach does not take into account the quivering energy of the departing electron in the laser field, which is $U_p = 6.0$ eV at $I = 10^{14}$ W/cm^2 and $\lambda = 800$ nm in linear polarization. The tunneling theories developed by Russian physicists in the 1960s constitute an alternative approach [6,7]. The most commonly used theory is the Ammosov-Delone-Kainov (ADK) approach, which is valid when the adiabaticity parameter γ is lower than 1 [8]. The parameter γ is the ratio between the tunneling time and the laser optical period, and is given by $\gamma = \omega\sqrt{2I_p}/F$, where ω and F are, respectively, the laser's angular frequency and electric field, and I_p is the ionization potential [6]. Atomic units (a.u.) are used in this section. The ADK model represents the limit when $\gamma \rightarrow 0$ of the theory proposed by Perelo-

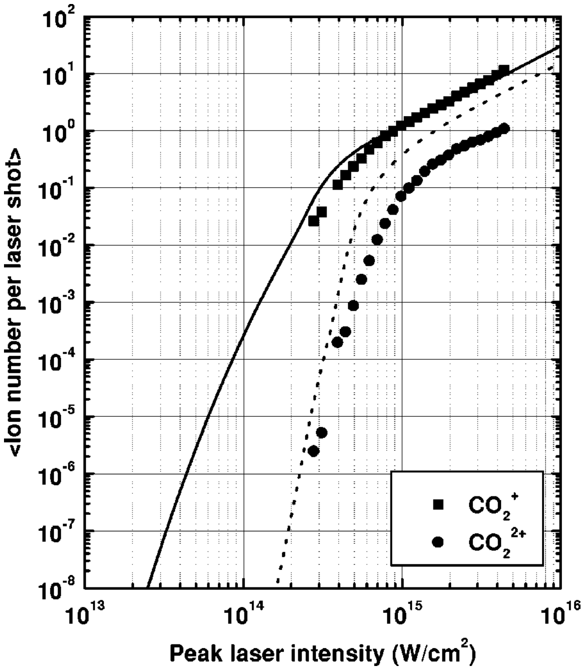

FIG. 5. Experimental (squares, CO_2^+ and circles, CO_2^{2+}) and calculated average ion numbers per laser shot for a reference pressure $p(CO_2) = 10^{-9}$ Torr as a function of the peak laser intensity for circularly polarized laser light. The model predictions are represented by the full curve (—) for single ionization and the dotted curve ($\cdots$) for sequential double ionization.

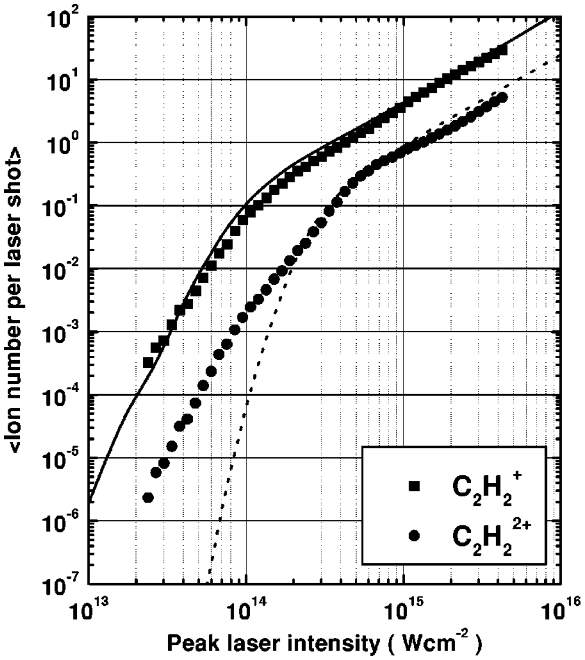

FIG. 6. Experimental (squares, $C_2H_2^+$ and circles, $C_2H_2^{2+}$) and calculated average ion numbers per laser shot for a reference pressure $p(C_2H_2) = 10^{-9}$ Torr as a function of the peak laser intensity for linearly polarized laser light. The model predictions are represented by the full curve (—) for single ionization and the dotted curve ($\cdots$) for sequential double ionization.

mov, Terent'ev, and Popov (PPT), which is valid for arbitrary γ values [7]. In fact, the ADK ionization rate given by Eq. (1) in Ref. [8] is derived *directly* from the PPT ionization rate using a $\gamma=0$ adiabaticity parameter. The comparison between the ADK and PPT predictions will be commented on in more detail in Sec. IV A.

The PPT model was developed using the Green-function formalism for levels bound by short-range forces and corrected for the long-range Coulomb interaction in order to be applied to the neutral and charged atoms ionization processes [28] . In this paper we use the rates given in Refs. [7,28] with the modifications described below. In the dipole coupling approximation, the ionization rates are established for electric fields $\mathbf{F}(t)$ with constant amplitude F following:

$$\mathbf{F}(t)=F[\cos(\omega t)\hat{\mathbf{x}}+\varepsilon\sin(\omega t)\hat{\mathbf{y}}], \tag{2}$$

where ω and ε are, respectively, the electric-field angular frequency and ellipticity ($\varepsilon=0$ for linear polarization and $\varepsilon=\pm 1$ for left and right circular polarizations).

For instance, the ionization rate $w_{\kappa\ell m}(F,\omega,\varepsilon=0)$ for the ionization of an atom or ion by a linearly polarized laser light is

$$\begin{aligned} w_{\kappa\ell m}&(F,\omega,\varepsilon=0)\\ &=\left(\frac{6}{\pi}\right)^{1/2}(3)^{2\nu-|m|-3/2}|E_\kappa||C_{\kappa\ell}|^2\\ &\quad\times\frac{(2\ell+1)(\ell+|m|)!}{2^{|m|}(|m|)!(\ell-|m|)!}\left(\frac{2F_\kappa}{3F}\right)^{2\nu-|m|-3/2}\\ &\quad\times(1+\gamma^2)^{(|m|/2)+(3/4)}A_m(\omega,\gamma)\\ &\quad\times\exp\left[-\frac{2F_\kappa}{3F}g_L(\gamma)\right]. \end{aligned} \tag{3}$$

In Eq. (3), ℓ and m represent the orbital and magnetic quantum numbers of the bound electron, and the momentum κ and effective principal quantum number ν are defined from the electron binding energy E_κ following $E_\kappa=-\kappa^2/2=-Z^2/(2\nu^2)$, where Z is the charge of the remaining core. The ratio F_κ/F plays a determinant role, where $F_\kappa=\kappa^3$ is the electric field experienced by the electron in its bound state. The factor $A_m(\omega,\gamma)$ is given in Eq. (56) of Ref. [7]. This factor takes into account the multiphoton absorption of the energy and in particular the fact that the minimal number of absorbed photons has to overcome the quivering energy of the departing electron in addition to its binding energy. The function $g_L(\gamma)$ as well as the ionization rates in circular polarization $\varepsilon=\pm 1$ are given in Ref. [7]. Finally the ionization rate given in Eq. (3) takes into account the Coulomb correction which introduces a factor $[(2F_\kappa/F)C(\gamma,\varepsilon)]^{2\nu}$, where $C(\gamma,\varepsilon)$ is a function of the adiabaticity parameter γ and laser ellipiticity ε, and is equal to 1 in linear polarization [28].

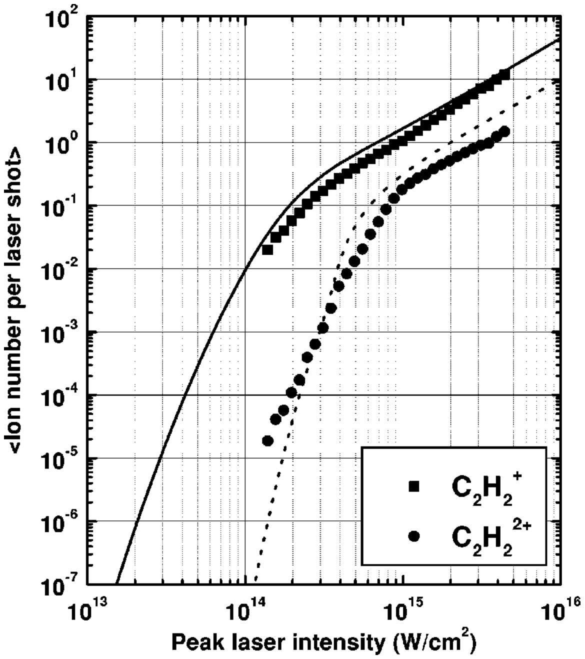

FIG. 7. Experimental (squares, $C_2H_2{}^+$ and circles, $C_2H_2{}^{2+}$) and calculated average ion numbers per laser shot for a reference pressure $p(C_2H_2)=10^{-9}$ Torr as a function of the peak laser intensity for circularly polarized laser light. The model predictions are represented by the full curve (—) for single ionization and the dotted curve ($\cdots$) for sequential double ionization.

B. Molecular single-ionization rates

The calculation of the ionization rate given in Eq. (3) is based on the asymptotic behavior of the wave function $\psi_{\kappa\ell m}(r,\vartheta,\varphi)$ when $\kappa r\gg 1$, where r is the radial coordinate of the electron:

$$\psi_{\kappa\ell m}(r,\vartheta,\varphi)\sim C_{\kappa\ell}\kappa^{3/2}(\kappa r)^{\nu-1}\exp(-\kappa r)Y_{\ell m}(\vartheta,\varphi). \tag{4}$$

In principle, the computation of $C_{\kappa\ell}$ requires the exact solution of the Schrödinger equation. Ammosov *et al.* give an approximation of this coefficient in the form $|C_{\kappa\ell}|^2=|C_{n^*\ell^*}|^2$ where $n^*=\nu$ and $\ell^*=\nu-1$ [8].

In the molecular case, the electronic potential is no more centrosymmetric. In the case of linear molecules, the electron wave function exhibits only one good quantum number λ, which is the projection of the orbital momentum along the internuclear axis in the molecular frame (Mol). The corresponding state vector $|\lambda\rangle_{\mathrm{Mol}}$ can be projected on the spherical-harmonics vector basis $|\ell\lambda\rangle_{\mathrm{Mol}}$ following:

$$|\lambda\rangle_{\mathrm{Mol}}=\sum_{\ell}|\ell\lambda\rangle_{\mathrm{Mol}}\times\langle\ell\lambda|\lambda\rangle_{\mathrm{Mol}}. \tag{5}$$

Since the calculation is performed in the laboratory frame (Lab) relative to the laser field properties, the state vector has to be expressed in this frame,

$$|\lambda\rangle_{\mathrm{Lab}}=\sum_{\ell m}|\ell m\rangle_{\mathrm{Lab}}D^{(\ell)}_{m\lambda}(\Omega)\langle\ell\lambda|\lambda\rangle_{\mathrm{Mol}}, \tag{6}$$

where $D^{(\ell)}_{m\lambda}(\Omega)$ is the matrix element of the $D^{(\ell)}$ representation of SO(3) in the spherical-harmonics vector basis and Ω represents the Euler angles between the molecular and laboratory frames.

In order to apply the atomic formalism, we assume that the molecular radial wave function $\langle r|\kappa\rangle_{\rm Mol}=\langle r|\kappa\rangle_{\rm Lab}$ behaves like the atomic one as in Eq. (4), since the wave function is essentially Coulombic when $\kappa r\gg 1$. In addition, the molecular ionization rate has to be averaged over all the directions of the molecular frame following $\int d\Omega\, \psi_{\kappa\lambda}\psi^*_{\kappa\lambda}/(8\pi^2)$ using the Green formalism of Perelomov *et al.* [7]. Due to the orthogonality properties of the $D^{(\ell)}_{mm'}$ matrices, the molecular ionization rate is expressed as a function of the atomic ionization rates $w_{\kappa\ell m}(F,\omega,\varepsilon)$ as follows:

$$w_{\kappa\lambda}(F,\omega,\varepsilon)=\sum_{\ell m}\frac{w_{\kappa\ell m}(F,\omega,\varepsilon)}{2\ell+1}|\langle\ell\lambda|\lambda\rangle_{\rm Mol}|^2. \qquad (7)$$

In our experiments, the ratio F_κ/F is always larger than 10 for laser intensities below the ionization saturation laser intensities. As a result only the $m=0$ component contributes noticeably to the ionization rate $w_{\kappa\lambda}(F,\omega,\varepsilon)$ because of the $(2F_\kappa/3F)^{-|m|}$ factor in Eq. (3). This $|m|$ dependence also occurs in circular polarization $\varepsilon=\pm 1$. Keeping only the term with $m=0$ in Eq. (7), the molecular ionization rate $w_{\kappa\lambda}(F,\omega,\varepsilon)$ can be expressed from the atomic ionization rate $w_{\kappa\ell m}(F,\omega,\varepsilon)$ replacing the factor $|C_{\kappa\ell}|^2[(2\ell+1)(\ell+|m|)!]/[2^{|m|}(|m|)!(\ell-|m|)!]$ with the molecular coefficient $|C_{\kappa\lambda}|^2$ given by

$$|C_{\kappa\lambda}|^2=\sum_{\ell}|C_{\kappa\ell}|^2|\langle\ell\lambda|\lambda\rangle_{\rm Mol}|^2. \qquad (8)$$

For instance, in linear polarization $(\varepsilon=0)$, the molecular single-ionization rate is

$$\begin{aligned}w_{\kappa\lambda}(F,\omega,\varepsilon=0)=&\left(\frac{6}{\pi}\right)^{1/2}(3)^{2\nu-3/2}|E_\kappa||C_{\kappa\lambda}|^2\\&\times\left(\frac{2F_\kappa}{3F}\right)^{2\nu-3/2}(1+\gamma^2)^{3/4}A_0(\omega,\gamma)\\&\times\exp\left[-\frac{2F_\kappa}{3F}g_L(\gamma)\right]. \qquad (9)\end{aligned}$$

C. Kinetic model for the sequential multiple ionization

Since the laser electric field is a pulsed field, the electric field amplitude F in Eq. (2) is replaced by a time-dependent field amplitude $Fg(t)$, where F is the maximum amplitude and $g(t)$ is the temporal envelope. The temporal evolution for the population n_Z of ion species of charge Z is given by

$$\frac{dn_{Z+1}}{dt}=w_{Z+1\leftarrow Z}n_Z-w_{Z+2\leftarrow Z+1}n_{Z+1}, \qquad (10)$$

where the ionization rates $w_{Z+1\leftarrow Z}$ are given in the preceding section as a function of $F\equiv Fg(t),\omega$, and ε. The integration in time is performed with a Gaussian envelope $g(t)$ which corresponds to a pulse duration of 50 fs (full-width at half maximum) relative to the laser intensity.

The populations obtained at the end of the laser pulse from Eq. (10) are convoluted to the spatial laser intensity distribution given in Eq. (1). Since the populations $n_Z(t=\infty)$ are computed as functions of the laser field F, it is easier to compute the total ion number N_Z following:

$$N_Z=\rho\int_0^{F_0}n_Z(t=\infty)dv(F), \qquad (11)$$

where ρ is the gas density, F_0 is the maximum laser electric field in the interaction volume, and $dv(F)$ is the spatial volume where the field strength is in between F and $F+dF$. Following the relationship between the laser intensity and laser electric field $I=\varepsilon_0 cF^2(1+\varepsilon^2)/2$ and Eq. (1), the volume $dv(f)$ where $F/F_0\in[f,f+df]$ is given by

$$dv(f)=\frac{2}{3}v_0\left(\frac{1}{f^2}-1\right)^{1/2}\left(\frac{1}{f^2}+2\right)\frac{df}{f}, \qquad (12)$$

where $v_0=\pi w_0^2 z_0/M^2$ is the elementary focal volume following the definitions given in Sec. II A. The measured laser beam parameters given in Sec. II A as well the gas density corresponding to a gas pressure $p=10^{-9}$ Torr at $T=298$ K are introduced in the calculations. Finally only the $Z=0,1,2$ populations are calculated and compared to the experimental results.

IV. RESULTS

A. Introduction to the experimental and calculated ion yields

The measured ion yields are presented in Figs. 1–7, where the experimental data are compared with the calculated ion yields from the sequential ionization model. The ion yields are plotted in log-log coordinates as a function of the peak laser intensity I_0 because of the nonlinear nature of the molecular response. The experimental and calculated ion yields exhibit the well-known saturation knee, and follow the $I_0^{3/2}$ intensity law above the saturation intensity. This behavior comes from the Gaussian geometry of the laser intensity reported in Eq. (1). When the peak laser intensity I_0 is much larger than the saturation intensity I_s, the number of detected ions N can be approximated by

$$N=\rho\int_{I_s}^{I_0}dv(I), \qquad (13)$$

where $dv(I)$ is the volume where the laser intensity is in between I and $I+dI$, and ρ is the gas density. This intensity distribution is linked to the field distribution given in Eq. (12) and the above equation gives

$$N=\rho v_0\left[W\left(\frac{I_0}{I_s}-1\right)\right]\approx\frac{2}{9}(\rho v_0)\left(\frac{I_0}{I_s}\right)^{3/2}, \qquad (14)$$

where v_0 is the elementary focal volume defined in Eq. (12). The $I_0^{3/2}$ intensity law appears from the leading term of the function $W(x)$ for $I_0 \gg I_s$. The exact form of this function is

$$W(x)=\frac{2}{9}x^{3/2}+\frac{4}{3}x^{1/2}-\frac{4}{3}\tan^{-1}(x^{1/2}). \tag{15}$$

The molecular ionization rates present one unknown parameter $C_{\kappa\lambda}$ defined in Eq. (8). The $C_{\kappa\ell}$ atomic factor can be calculated from quantum defect theory using the wave-function normalization constants given by Greene *et al.* [29],

$$C_{\kappa\ell}=\frac{2^{\nu}(-1)^{n-\ell-1}}{\left[\left(1+\frac{d\mu}{d\nu}\right)\nu\Gamma(\nu+\ell+1)\Gamma(\nu-\ell)\right]^{1/2}}. \tag{16}$$

The energy of the bound electron, $E_\kappa=-\kappa^2/2=-Z^2/(2\nu^2)$, is a function of the quantum defect μ defined by $\nu=n-\mu$. For $\mu=0$, Eq. (16) gives the usual asymptotic behavior of the hydrogenic wave functions. For complex atoms, Ammosov *et al.* give an approximation of this coefficient following [8]

$$|C_{\kappa\ell}|^2=|C_{n^*\ell^*}|^2=\frac{2^{2n^*}}{n^*\Gamma(n^*+\ell^*+1)\Gamma(n^*-\ell^*)}, \tag{17}$$

where $n^*=\nu$ and $\ell^*=\nu-1$.

The molecular behavior is introduced with the coefficients $|\langle\ell\lambda|\lambda\rangle_{\mathrm{Mol}}|^2$ in Eq. (8) for the $|C_{\kappa\lambda}|^2$ molecular coefficient. These quantities depend on molecular orbitals and can be computed only from *ab initio* wave-function calculations. The method chosen in this paper is to introduce the ADK atomic coefficient $|C_{n^*\ell^*}|^2$ in the ionization rates of the neutral and singly charged molecules, with the corresponding ionization potentials. Then a corrective factor is applied to these coefficients in order to get the experimental singly charged ion yields above the laser saturation intensity. Following the previous notations, this coefficient is equal to $|C_{\kappa\lambda}/C_{n^*\ell^*}|^2$. For each molecular species, the same coefficient is introduced in the ionization rates of neutral and singly charged molecules in order to use only one parameter, and remains unchanged in linear and circular polarization since it depends only on the asymptotic behavior of the electronic wave function. Its significance is linked to the molecular behavior in comparison with the atomic one and will be commented in the next section after the presentation of the experimental results. Table I gives these corrective molecular coefficients for N_2, CO_2, C_2H_2, and C_3H_4. This correction procedure is chosen because of the widely used ADK $|C_{n^*\ell^*}|^2$ coefficients for atoms. However, this coefficient remains an approximation. For instance, for atomic hydrogen in its 1*s* ground state, the ADK approximation of $|C_{\kappa\ell}|^2=|C_{n=1,\ell=0}|^2=4$ is $|C_{n^*=1,\ell^*=0}|^2=4.70$ from Eq. (20) in Ref. [8] taking into account a typographical error , while a better approximation of Eq. (17) gives $|C_{n^*=1,\ell^*=0}|^2=4.17$. Now let us consider the oxygen atom that exhibits an ionization potential 13.6 eV close the hydrogen ionization potential. Following the ADK approximation, these two species will have very close $|C_{n^*\ell^*}|^2$ coefficients. However, this coefficient has to depend on the asymptotic behavior of the electronic wave function. To our knowledge, hydrogen and oxygen atoms do not exhibit similar wave functions due to their respective 1*s* monoelectronic character in hydrogen and $2p^4$ multielectronic character in oxygen.

TABLE I. Corrective molecular coefficients $|C_{\kappa\lambda}/C_{n^*\ell^*}|^2$ introduced in the ionization rates. See text for the C_3H_4 molecular corrective coefficient interpretation.

Molecule	$\lvert C_{\kappa\lambda}/C_{n^*\ell^*}\rvert^2$
N_2	0.5
CO_2	0.3
C_2H_2	0.14
C_3H_4	0.08

Finally, the PPT model is compared to the more widely used ADK model in Fig. 8, which represents the ion yields for He, N_2, and C_2H_2 using the PPT and ADK ionization rates. In both cases, the ADK parameters $|C_{n^*\ell^*}|^2$ are used. As expected from the validity of the ADK model, the disagreement between the two models predictions is more pronounced for species with lower ionization potentials such as C_2H_2 $[I_p(C_2H_2)=11.4\ \mathrm{eV}]$ in comparison with helium $[I_p(\mathrm{He})=24.6\ \mathrm{eV}]$. This behavior is linked to the value of the γ parameter, which is plotted in Fig. 9. For helium, the ionization takes place above 10^{14} W/cm^2, where the γ pa-

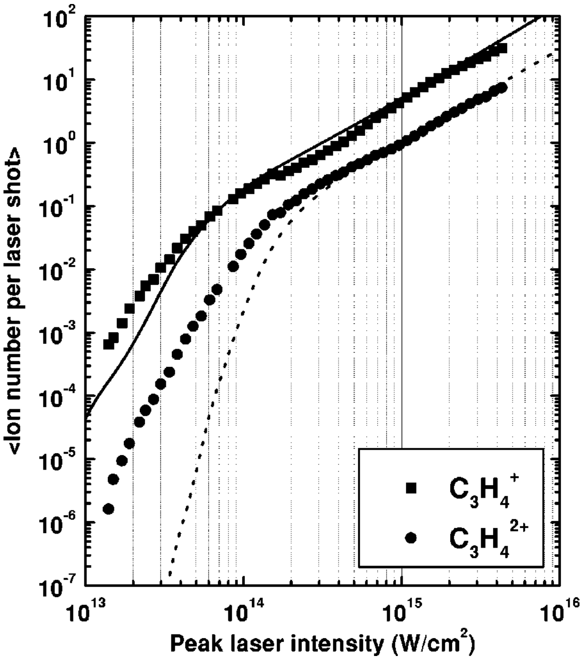

FIG. 8. Experimental (squares, $C_3H_4{}^+$ and circles, $C_3H_4{}^{2+}$) and calculated average ion numbers per laser shot for a reference pressure $p(C_3H_4)=10^{-9}$ Torr as a function of the peak laser intensity for linearly polarized laser light. The model predictions are represented by the full curve (—) for single ionization and the dotted curve (· · ·) for sequential double ionization.

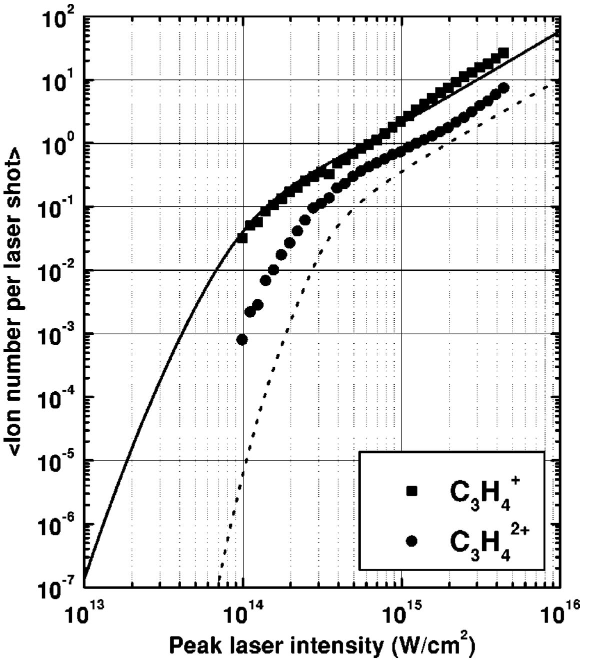

FIG. 9. Experimental (squares, $C_3H_4^+$ and circles, $C_3H_4^{2+}$) and calculated average ion numbers per laser shot for a reference pressure $p(C_3H_4)=10^{-9}$ Torr as a function of the peak laser intensity for circularly polarized laser light. The model predictions are represented by the full curve (—) for single ionization and the dotted curve $(\cdots)$ for sequential double ionization.

rameter remains close or smaller than 1. On the contrary for N_2 and C_2H_2, the ionization takes place below 10^{14} W/cm^2, where the γ parameter is significantly larger than 1. In this intensity range, the ADK model is no more valid. Even for helium, the disagreement between the PPT and ADK rates increases at lower laser intensities as it is expected. At laser intensities above saturation, the PPT ion yields are higher than the ADK rates, especially when the ionization potential gets lower. This is due to the laser intensity distribution within the focal volume. Indeed, since the PPT rates are higher than the ADK rates at low laser intensity, the extension of the focal volume will contribute to the total ion yield more significantly in the PPT model. In the following sections, the measured ion yields are compared only to the PPT calculated ion yields for the sake of clarity in Figs. 1–7. Moreover, the validity of the PPT model was clearly established for rare-gas atoms by Larochelle *et al.* [11].

B. N_2

Some of the N_2 results have been presented in a previous paper in comparison with an atomiclike ADK sequential-ionization model [4]. Figure 1 represents the N_2^+, N_2^{2+}, and the sum of the N_2^{2+} and N^+ ion yields in comparison with the tunneling model predictions presented in this paper. In Ref. [4], it was shown that the detected N_2^{2+} ions and $N^++N^++E_{\text{Kinetic}}$ fragmentation channels follow the same laser intensity dependence for different kinetic energy releases E_{Kinetic}. The kinetic-energy release spectrum of the N^++N^+ channels takes place in the 5–13-eV range with a maximum at 7.6 eV. It was concluded that these ion species belong to two different decay channels of the $[N_2^{2+}+2e^-]$ complex after the laser excitation following

$$[N_2^{2+}+2e^-]\rightarrow N_2^{2+}+2e^-, N^++N^++2e^-. \quad (18)$$

In Fig. 1 the total contribution of the molecular double ionization is the sum of the N_2^{2+} and N^+ ion yields, where the N^+ ions belong to the $N^++N^++E_{\text{Kinetic}}$ (5.6 eV$\leqslant E_{\text{Kinetic}}\leqslant$11.6 eV) channels identified from the ion-ion correlation technique. Using a molecular corrective factor $|C_{\kappa\lambda}/C_{n^*l^*}|^2=0.5$, the PPT model gives a better agreement than the ADK model for the N_2^+ ion yield, since all the measured ion yields lie on the PPT calculated curve (see Fig. 8 for a comparison of ADK and PPT rates). Moreover, using the same corrective coefficient, the saturation intensity of the (N_2^{2+},N^++N^+) contribution is well reproduced.

Below the saturation intensity, the sequential model cannot reproduce the ion yields from the double-ionization decay channels. As in the case of atoms, this is a clear signature of nonsequential double ionization below the saturation intensity of the single-ionization process. Since the N_2^{2+} detected dications are produced at short internuclear distance, where covalent forces are effective, the double-ionization process is a vertical Franck-Condon excitation [4]. Another example of this behavior will be given for the CO_2 molecule. Experiments were not performed using circular polarization because the N_2^{2+} signal occurs at the same time of flight as the N^+ ions ejected perpendicularly to the spectrometer axis. In this case, it is not possible to separate the N_2^{2+} contribution from the N^+ contribution.

C. CO_2

Figure 2 represents the CO_2 results recorded using linearly polarized laser light. The molecular corrective coefficient is $|C_{\kappa\lambda}/C_{n^*l^*}|^2=0.3$. The agreement with the experimental data is less satisfactory than in the N_2 case. In particular, below the CO_2^+ laser saturation intensity, the measured CO_2^+ ion yields are smaller than the calculated ones. The ionization potential, $I_p(CO_2^+:\tilde{X}^2\Pi_g \leftarrow CO_2:\tilde{X}^1\Sigma_g^+)=13.77$ eV, corresponds to the ionization process leading to the $\tilde{X}^2\Pi_g$ electronic ground state of the CO_2^+ ion. Ionization leading to excited states of CO_2^+, for instance $\tilde{A}^2\Pi_u$ or $\tilde{B}^2\Sigma_u^+$, involves higher ionization potentials $I_p(CO_2^+:\tilde{A}^2\Pi_u \leftarrow CO_2:\tilde{X}^1\Sigma_g^+)=17.30$ eV and $I_p(CO_2^+:\tilde{B}^2\Sigma_u^+ \leftarrow CO_2:\tilde{X}^1\Sigma_g^+)=18.06$ eV. Following Eq. (3), higher ionization potentials will lower the ionization rate because of the exponential factor $\exp[-2F_\kappa g_L(\gamma)/3F]$, where $F_\kappa=\kappa^3=(2I_p)^{3/2}$. Consequently, the differences observed in Fig. 2 between the CO_2^+ measured and calculated ion yields might be the signature of final excited states of the CO_2^+ ion. However, since the exact contribution of these states is not known, no trials were undertaken to introduce their energies in the calculation. As in the N_2 case, the CO_2^{2+} and O^++CO^+ double-ionization decay channels follow the same laser intensity dependence at low intensity because they come from the same complex $[CO_2{}^{2+}+2e^-]$ as in the following:

$$[CO_2{}^{2+}+2e^-]\rightarrow CO_2{}^{2+}+2e^-, O^+ + CO^+ + 2e^-. \tag{19}$$

Above saturation, the total contribution of these decay channels is not reproduced by the calculation using the same molecular corrective coefficient as for the neutral CO_2 ionization. However, although the sequential ionization model overestimates the double-ionization signals, the measured ion yields are several orders of magnitude larger than the predicted ones at low laser intensities. As in the N_2 case, this fact is a clear signature of nonsequential double ionization,

$$CO_2+\text{laser}\rightarrow[CO_2{}^{2+}+2e^-]. \tag{20}$$

For laser intensities above the $CO_2{}^+$ saturation intensity, the double ionization is sequential because only $CO_2{}^+$ ions occupy the laser focal volume. In this intensity range, the $CO_2{}^{2+}$ ion yield does not follow the $I_0^{3/2}$ saturation law. This might be due to further ionization and/or dissociation of this ion by the laser field. On the contrary, the $I_0^{3/2}$ saturation law is observed for the $O^+ + CO^+$ channel laser intensity dependence, which is not represented in Fig. 2 for sake of clarity. Concerning the discrepancy with the calculations above the saturation intensity where single ionization is effective, the ionization potential of $CO_2{}^+$ introduced in the ionization rate is $I_p(CO_2{}^+)=22.4$ eV, and the observed difference between the experimental and calculated ion yields might be due to the fact that the ionization of $CO_2{}^+$ produces excited states of the $[CO_2{}^{2+}]$ complex. In this case, the ionization potential is higher than 22.4 eV, and the ionization rate is lower.

Figure 3 presents the measured and calculated ion yields in circular polarization. Above the saturation intensity of the $CO_2{}^+$ ion species, the $CO_2{}^+$ ion yields are well-reproduced by the calculation using the same corrective coefficient as in linear polarization. This feature is expected from our model, since the corrective factor depends only on the molecular orbitals, and is independent of the laser polarization state. Below the $CO_2{}^+$ saturation intensity, the model overestimates the ion yields. As in the linear case, this might be the signature that the ionization of neutral molecules does not occur only via the fundamental sate of $CO_2{}^+$, but also via excited states of the ion. For the double-ionization channels, only the $CO_2{}^{2+}$ ion yields are reported because it is difficult to separate in the time-of-flight spectrum the contribution of the $O^+ + CO^+$ channels with a specified kinetic energy release, since the fragmentation is isotropic in the plane of the circularly polarized laser light. Above the $CO_2{}^{2+}$ saturation intensity, the calculated ion yields are five times larger than the $CO_2{}^{2+}$ yields. This large difference comes from the fact that the fragmentation channels are not taken into account as in the linear case, while the calculation concerns all the double-ionization decay channels. Below the saturation intensity, the signature of nonsequential double-ionization remains difficult to assign, since the measured ion yields remain below the predicted sequential ion yields.

D. C_2H_2

Figure 4 presents the measured and calculated ions yields for the C_2H_2 molecule in linear polarization. The saturation knees of $C_2H_2{}^+$ at $I_s(C_2H_2{}^+)\approx 10^{14}$ W/cm^2 and $C_2H_2{}^{2+}$ at $I_s(C_2H_2{}^{2+})\approx 3\times10^{14}$ W/cm^2 are well reproduced by the sequential calculation for a molecular corrective factor 0.14. The overall $C_2H_2{}^+$ experimental data are in good agreement with the PPT model. For the $C_2H_2{}^{2+}$ ion, three laser intensity ranges bounded by $I_s(C_2H_2{}^+)\approx 10^{14}$ W/cm^2 and $I_s(C_2H_2{}^{2+})\approx 3\times10^{14}$ W/cm^2 appear in Fig. 4. For $I>I_s(C_2H_2{}^{2+})$, the double ionization is sequential since the data are reproduced by the calculation. For $I_s(C_2H_2{}^+)<I<I_s(C_2H_2{}^{2+})$, an increasing disagreement is observed when the laser intensity I is decreased. In this laser intensity range, nonsequential double ionization begins to be effective. Finally for $I<I_s(C_2H_2{}^+)$, the disagreement is a clear signature of nonsequential double ionization. A saturation knee appears for $C_2H_2{}^{2+}$ ions at the same intensity $I_s(C_2H_2{}^+)\approx 10^{14}$ W/cm^2 as for $C_2H_2{}^{2+}$ ions. The reason is that the direct double ionization of neutral molecules saturates at the the same intensity as the single ionization, because there are no more neutral species in the interaction volume.

The molecular ion yields in the intermediate region, $I_s(C_2H_2{}^+)<I<I_s(C_2H_2{}^{2+})$, exhibit a similar behavior as in atomic helium [10], but with a much less observable passage from the nonsequential regime to the sequential regime. In the helium case, the saturation knees for the single and nonsequential double ionizations of neutral atoms appear clearly before the saturation knee of the ionization of singly charged He^+ ions. The two separated well-defined knees of the He^{2+} ion yields are due to the fact that the laser intensity has to be increased significantly to ionize the He^+ ion. In the C_2H_2 case, the ionization potential of $C_2H_2{}^+$ ions is 20.3 eV and is much lower than the 54.4-eV ionization potential of He^+. Consequently, the saturation intensities of the single ionizations of the neutral and singly charged molecule are closer than in the helium case. This overall behavior can be observed with N_2 and CO_2, basically for the same reasons.

Two missing electron fragmentation channels such as $H^+ + C_2H^+$ or $CH^+ + CH^+$ are not detected. Indeed the good agreement between the detected $C_2H_2{}^{2+}$ dication ion yields and the results of the calculation above the saturation laser intensity $I_s(C_2H_2{}^{2+})$ gives another indication that these channels play a minor role, since the calculation includes all the decay channels from the single ionization of $C_2H_2{}^+$ ions. The circular polarization results are presented in Fig. 5. Using the same molecular corrective factor as in linear polarization, a relative good agreement is obtained only for $C_2H_2{}^+$ ions. Unlike the linear case, the calculation overestimates the $C_2H_2{}^{2+}$ ion yields above saturation. Below saturation, the crossing of the calculated and experimental $C_2H_2{}^{2+}$ ion-yield curves might be an indication for nonsequential ionization in circular polarization, but with a much less pronounced behavior than in linear polarization.

E. C_3H_4

The analysis of Fig. 6 and Fig. 7 gives the same conclusions as for the other molecules. In linear polarization, the

$C_3H_4{}^{2+}$ ion yields exhibit a single saturation knee because of the low ionization potential, $I_p(C_3H_4{}^+)=18$ eV, of the $C_3H_4{}^+$ ion. Consequently, the intermediate region from nonsequential to sequential behaviors does not appear, as in the helium case [10]. In addition, the slight fluctuations of the measured ion yields around the calculated curve above saturation might indicate the presence of resonances. In circular polarization, the agreement is obtained only for the singly charged $C_3H_4{}^+$ ions. Although the calculation overestimates the $C_3H_4{}^{2+}$ ion yields, the overall parallelism of the experimental and calculated curves show that the double ionization is dominated by sequential processes.

In the time-of-flight spectra, $C_3H_3{}^+$ and $C_3H_2{}^{2+}$ ions are also detected with a weaker contribution than the $C_3H_4{}^+$ and $C_3H_4{}^{2+}$ ions. These ions come from fragmentation channels involving hydrogen atoms and protons. For instance, $C_3H_2{}^{2+}$ dications might come from a proton loss from $C_3H_3{}^+$, and also from a hydrogen atom loss from $C_3H_3{}^{2+}$ dications that appear very weakly in the time-of-flight spectra. Due to the complicated dynamics for these ions production, they are not taken into account for a first approach of double ionization of C_3H_4. Consequently, the molecular corrective coefficient reported in Table I has a weaker meaning than for other molecules, where the double-ionization fragmentation channels were clearly identified.

V. DISCUSSION

In this section the validity of the molecular single-ionization rates is discussed in comparison with the experimental data. The comparison applies to the ionization of neutral molecules, and to the ionization of single charged molecules in the laser intensity range where nonsequential double ionization is no more effective, i.e., above the laser saturation intensity of the neutral species. The nonsequential double-ionization results are compared with the predictions of the rescattering model in order to emphasize the need for a full quantum approach of this process.

A. Single ionization of neutral molecules

A reasonable agreement is obtained between the measured singly charged molecules ion yields and the model predictions developed in Sec. III. The molecular corrective coefficients are given in Table I from the experimental measurements, and find their origin in Eq. (8). These corrective coefficients are smaller than 1, and decrease as the sizes of the molecules increase. Let us emphasize that this an experimental conclusion which has to be considered in the frame of the chosen ionization model developed in Sec. III B. In particular, the molecular ionization rates are obtained using an atomic pointlike radial dependence of the electronic wave function at large r, $\psi_{\mathrm{Rad},\kappa}(r)\sim\kappa^{3/2}(\kappa r)^{\nu-1}\exp(-\kappa r)$, but with a molecular angular dependence to take into account the fact that the atomic orbital quantum number ℓ is no longer a good quantum number for molecules. This angular dependence introduces the anisotropy of the molecular field. In Eq. (8), the $C_{\kappa\lambda}$ coefficient is built with different atomic $C_{\kappa\ell}$ values, which decrease as ℓ increases. For instance, for pure hydrogenic wave functions where $\kappa=Z/n$, the ratio $|C_{\kappa\ell}/C_{\kappa,\ell+1}|^2$ is given by

$$\left|\frac{C_{\kappa\ell}}{C_{\kappa,\ell+1}}\right|^2=\frac{n+\ell+1}{n-\ell-1}. \tag{21}$$

Since the atomic $|C_{\kappa\ell}|$ and the associated ADK $|C_{n*\ell*}|$ coefficients involve the lowest possible ℓ value, they are larger than the molecular $|C_{\kappa\lambda}|$ coefficient. This does not mean that molecules are harder to ionize than atoms, because the main contribution in the ionization rate comes from the momentum κ associated with the ionization potential $E_\kappa=-\kappa^2/2$. For instance, molecules such as CO_2 or C_2H_2 have lower ionization potentials than atoms such as He, Ne, or Ar. Consequently, the corresponding molecular ionization rates are higher than the atomic ionization rates.

For the simplest investigated molecule N_2, the corrective coefficient is $|C_{\kappa\lambda}/C_{n*\ell*}|^2=0.5$. Following the above discussion, the $|C_{\kappa\lambda}|$ is around $\sqrt{2}$ smaller for the N_2 $3\sigma_g$ outermost orbital than for an ADK atomic orbital. This result is in good agreement with the results of Liang *et al.*, who found that the Ar^+ ion yields are larger than the $N_2{}^+$ ion yields [30]. The choice of the atomic argon for the comparison was due to the close ionization potentials of Ar, $I_p(\mathrm{Ar})=15.75$ eV, and N_2,$I_p(N_2)=15.58$ eV. The decrease of the corrective coefficient in Table I as a function of the investigated molecules might be due to several effects. The first one has to be associated to the molecular electronic configuration. In N_2, the outer shell is built with σ_g electrons, while other molecular species involve π electrons. In a recent work of Guo *et al.*, the O_2 ionization rates were found very weak in comparison with the atomic xenon ionization rates [31]. Considering the comparisons of, respectively, N_2 and Ar, and O_2 and Xe, these authors concluded that electronic structure plays a significant role in tunnel ionization. However, unlike O_2, the molecules reported in Table I exhibit closed-shell electronic structures as rare-gas atoms. Another reason for the decrease of the corrective coefficient might be linked to the size of the molecule. The molecular electronic wave function is increasingly different from an atomic wave function, and the $|C_{\kappa\lambda}|^2$ development in Eq. (8) involves higher ℓ values as the molecular size increases. The molecular corrective coefficient reported for C_3H_4 in Table I is a less accurate value than for other molecules, since the fragmentation channels involving $C_3H_3{}^+$ and $C_3H_2{}^{2+}$ are not taken into account. The effective coefficient is thus expected to be larger and might be closer to the C_2H_2 coefficient.

Finally, the molecular reorientation is not taken into account in this discussion. In Sec. III B, the ionization rate is calculated assuming an isotropic molecular distribution. In our opinion, this problem remains to be investigated in more detail, but is not straighforward since different molecular orientations can contribute to the total ion signal at different times during the laser pulse. Consequently, a theoretical approach including the electronic *and* nuclear dynamics in tractable analytical ionization rates is still missing. Nevertheless, the contribution of reorientation processes might be included in the experimental molecular corrective coefficients given in Table I.

B. Single ionization of singly charged molecules

The same corrective coefficients were applied to the ionization rates of neutral and singly charged molecules in order to introduce only one parameter per molecule. This approximation can be justified by the fact that the outermost orbitals of the neutral and singly charged molecular electronic ground states exhibit the same symmetries for N_2, CO_2, C_2H_2, and C_3H_4. For instance, they are $\ldots 1\pi_u^4\ 3\sigma_g^2$ and $\ldots 1\pi_u^4\ 3\sigma_g$ in, respectively, N_2 and $N_2{}^+$, and $\ldots 1\pi_u^4\ 1\pi_g^4$ and $\ldots 1\pi_u^4\ 1\pi_g^3$ in, respectively, CO_2 and $CO_2{}^+$. In linear polarization, the agreement with the experimental data is good for N_2, C_2H_2, and C_3H_4, in the laser intensity range where the sequential ionization is effective, i.e., above the saturation intensity of the neutral species. In all other cases except for CO_2 in circular polarization, the disagreement does not exceed a factor of 2. Finally, the CO_2 disagreement in circular polarization come from the fact that the $O^+ + CO^+$ contribution is not taken into account in the comparison with the predictions of the calculation.

These results show that the $|C_{\kappa\lambda}|^2$ coefficients are not very different for neutral and singly charged molecules, although the corresponding wave functions are not identical because of the different electronic potentials of the neutral and singly charged molecules. In conclusion, for a better understanding of single ionization of neutral and singly charged molecules, a detailed knowledge of the final states of the ionization process is necessary as it is outlined for CO_2 in Sec. IV C. Electron spectroscopy might be quite helpful for the determination of these states as well as for the investigation of the correlated dynamics of the two electrons ejected at low laser intensities where nonsequential double ionization plays a dominant role.

C. Nonsequential double-ionization rates

Nonsequential double ionization was established using the comparison between the experimental data and a sequential ionization model. Another way is to consider the ratio between the detected products of double-and single-ionization processes [10]. For laser intensities well below the single-ionization saturation intensity, the populations n_0, n_1, and n_2 of, respectively, the neutral species, singly, and doubly charged species follow the set of equations:

$$\frac{dn_0}{dt} = -(w_{20}+w_{10})n_0 \approx 0,$$

$$\frac{dn_1}{dt} = -w_{21}n_1 + w_{10}n_0 \approx w_{10}n_0, \qquad (22)$$

$$\frac{dn_0}{dt} = w_{21}n_1 + w_{20}n_0 \approx w_{20}n_0,$$

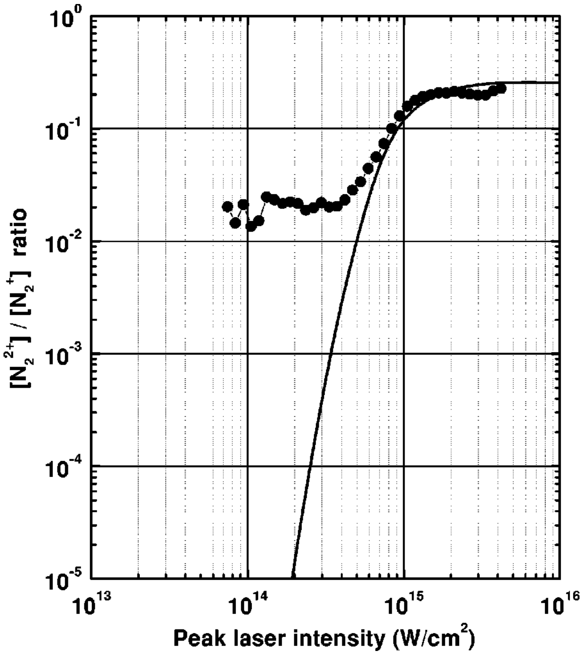

FIG. 10. Experimental (●) and calculated (—) ion signal ratios $[N_2{}^{2+}]/[N_2{}^+]$ as a function of the peak laser intensity for linearly polarized laser light.

for a fixed laser field, and where the rates w_{ji} represent the ionization from i to j species. In particular, the unknown w_{20} nonsequential double-ionization rate is included in the above kinetic equations. For a square temporal profile of the laser pulse, the n_2/n_1 ratio is given by $n_2/n_1 = w_{20}/w_{10}$ at the end of the laser interaction. As is expected, the ratio n_2/n_1 is very weak in the absence of nonsequential double ionization.

Figure 10 represents the measured $[N_2{}^{2+}]/[N_2{}^+]$ ratio, including the total contribution of double ionization in comparison with the prediction of the sequential model. For laser intensities below 4×10^{14} W/cm^2, the contribution of nonsequential double ionization shows that the ratio w_{20}/w_{10} does not vary significantly with the laser intensity. For laser intensities above 7×10^{14} W/cm^2, the agreement with the sequential model is good since double ionization is essentially sequential in this intensity range. This type of comparison no longer involves the unknown $C_{\kappa\lambda}$ coefficients and allows us to compare the laser intensity dependences of w_{10} and w_{20}. However, the measured ion yields come from the total distribution of the laser intensity within the focal volume.

The same comparisons are presented for C_2H_2 in Figs. 11 and 12 for, respectively, linearly and circularly polarized laser light. For linearly polarized laser light, the ratio w_{20}/w_{10} varies smoothly with the laser intensity and decreases for lower laser intensities. For circularly polarized laser light, the experimental curve crosses the sequential curve at $I \approx 4 \times 10^{14}$ W/cm^2. As outlined in Sec. IV D, this might be the signature of nonsequential double ionization in circular polarization. To our knowledge, no simple analytical expressions of w_{20} have been proposed in the literature for atoms and molecules. Consequently, the results in Figs. 10 and 11 might be helpful for a tunneling model of nonsequential double ionization.

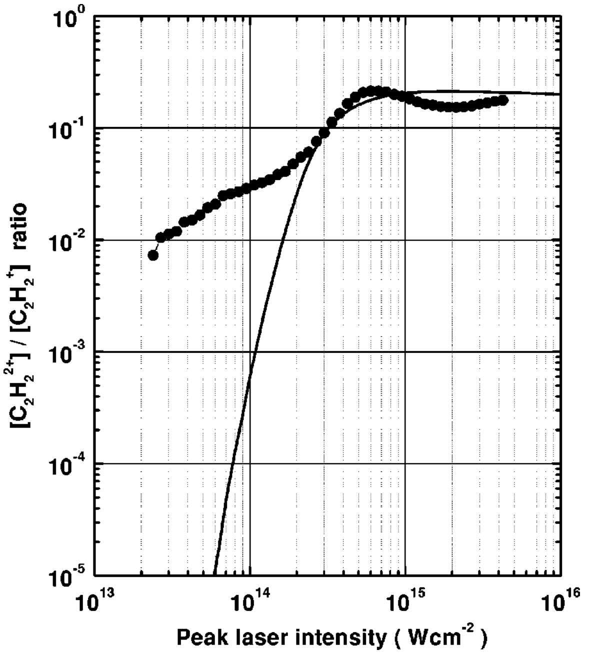

FIG. 11. Experimental (●) and calculated (—) ion signal ratios $[C_2H_2^{2+}]/[C_2H_2^{+}]$ as a function of the peak laser intensity for linearly polarized laser light.

D. Electron rescattering processes in nonsequential double ionization

The rescattering model was introduced by Corkum in order to explain a wide variety of strong fields effects, where the first ionized electron oscillates in the intense laser field [16]. According to this model, nonsequential double ionization is due to the return of the electron wave packet in the vicinity of the ion core. If the kinetic energy of the electron exceeds the e-$2e$ scattering energy, then the ion can be collisionaly ionized. This picture is very attractive since nonsequential double ionization is mainly observed in linearly polarized laser fields. Indeed for circularly polarized laser light, the electron trajectory never returns to the vicinity of the ion and the electron-ion interaction does not occur.

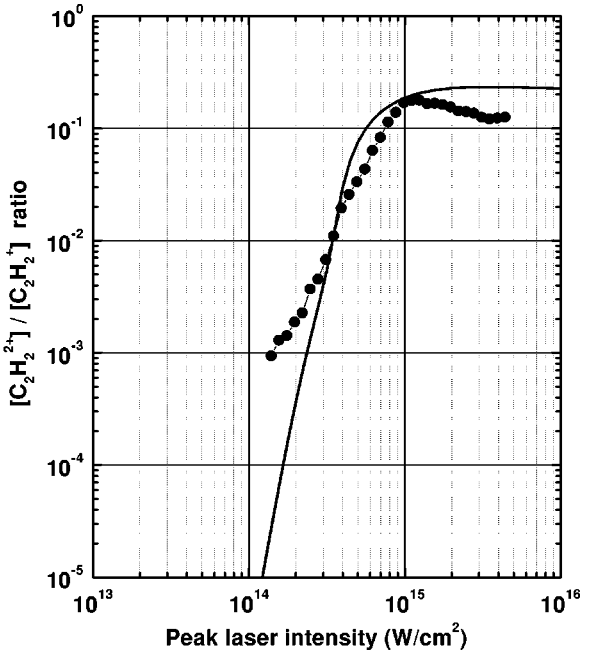

FIG. 12. Experimental (●) and calculated (—) ion signal ratios $[C_2H_2^{2+}]/[C_2H_2^{+}]$ as a function of the peak laser intensity for circularly polarized laser light.

TABLE II. Experimental appearance laser intensity for the dication $I_a(M^{2+})$, maximum electron return kinetic energy in linear polarization $3.17U_p[I_a(M^{2+})]$, and ionization potential of the singly charged molecule $I_p(M^{2+}\leftarrow M^{+})$ as functions of the molecule M.

Molecule M	$I_a(M^{2+})$ (W/cm^2)	$3.17U_p[I_a(M^{2+})]$ (eV)	$I_p(M^{2+}\leftarrow M^{+})$ (eV)
N_2	7×10^{13}	13.3	27.1
CO_2	5×10^{13}	9.5	22.4
C_2H_2	2×10^{13}	3.8	20.3
C_3H_4	10^{13}	1.9	18.0

In a linearly polarized electric field $\mathbf{F}(t)=\hat{\mathbf{x}}F\cos(\omega t)$, an electron ejected by a tunneling process will oscillate with an initial velocity $v(t_0)\approx 0$ at time t_0 when it is freed from the neutral molecule. The ponderomotive energy $U_p=q_e^2F^2/(4m_e\omega^2)$ is the average kinetic energy of the oscillating electron. The maximum kinetic energy in a rescattering process with the ion core is $T_{\max}=3.17U_p$ for an electron ejected at $\omega t_0=17°$ *modulo* 180°. Table II reports these maximum kinetic energies calculated at the appearance of laser intensities at $\lambda=800$ nm for the different detected dications. It is important to emphasize that these intensities are not significant physical quantities, but are simply related to the experimental method. In particular, they depend on the acquisition time because of the probabilistic nature of double ionization. In Table II the maximum return kinetic energies are smaller than the ionization potentials of singly charged molecules and, consequently, a direct e-$2e$ process cannot be responsible for nonsequential ionization at low laser intensity. However, in the case of N_2 and CO_2, the rescattering energies are sufficiently large to produce inelastic scattering leading to excited ionic states. Since the ionization rates of excited states are larger than the ionization rate of the fundamental state, inelastic scattering might be effective in molecular nonsequential double ionization. In the case of C_2H_2 and C_3H_4, the maximum rescattering energy remains in the electron volt range. In this case, the rescattering picture is more difficult to apply.

As outlined by Corkum, Watson *et al.*, and other researchers, a full quantum approach is necessary to investigate nonsequential double ionization of atoms and molecules [16,2,14,15,21]. In the molecular case, the one-dimensional model of Pegarkov *et al.* developed for N_2 is in good agreement with the experimental data of this paper [21]. Moreover, the correlated behavior of the ejected electrons in the atomic and molecular multiionization remains an important issue in strong laser fields physics. In particular, we already reported the nonsequential double ionization of CO_2^{+} ions leading to the multifragmention of the system into three singly charged atomic ions following [27]

$$CO_2{}^{+} + \text{laser} \rightarrow O^{+} + C^{+} + O^{+} + 2e^{-}. \tag{23}$$

To our knowledge, there is not yet a thorough understanding of these processes that might play quite a significant role in molecular multiionization and multifragmentation.

VI. CONCLUSION

Nonsequential double ionization of several molecules in strong laser fields has been unambiguously identified from the ion-yield measurements in comparison with a sequential ionization model. This effect is observed mainly using linearly polarized laser light. In circular polarization, nonsequential double ionization might be present, for instance for the C_2H_2 molecule, but with a much lower contribution than in linear polarization. The validity of a single-ionization tunneling model developed for atoms has been extended to molecules, and a relative good agreement is observed in laser intensity ranges, where single-ionization processes take place. Let us mention the case of the CO_2 molecule, which does not fit the predictions of the model, and consequently shows that the single ionization of molecules in strong laser fields demands further experimental and theoretical contributions. Finally, the first theoretical efforts aimed at the nonsequential double ionization of molecules appeared quite recently, and they constitute a promising challenge for the comparison of the experimental and theoretical results.

ACKNOWLEDGMENTS

The authors are pleased to acknowledge G. Vigneron (CEA/SCM) for his expertise of the kHz titaniums-sapphire laser system and M. Bougeard and E. Caprin (CEA/SPAM) for their skilled technical assistance.

[1] A. L'Huillier, L.A. Lompré, G. Mainfray, and C. Manus, J. Phys. B **16**, 1363 (1983).
[2] J.B. Watson, A. Sanpera, D.G. Lappas, P.L. Knight, and K. Burnett, Phys. Rev. Lett. **78**, 1884 (1997).
[3] A. Talebpour, S. Larochelle, and S.L. Chin, J. Phys. B **30**, L245 (1997).
[4] C. Cornaggia and Ph. Hering, J. Phys. B **31**, L503 (1998).
[5] Y. Gontier and M. Trahin, Phys. Rev. A **7**, 1899 (1973).
[6] L.V. Keldysh, Zh. Éksp. Teor. Fiz. **47**, 1945 (1964) [Sov. Phys. JETP **20**, 1307 (1965)].
[7] A.M. Perelomov, V.S. Popov, and M.V. Terent'ev, Zh. Éksp. Teor. Fiz. **50**, 1393 (1966) [Sov. Phys. JETP **23**, 924 (1966)].
[8] M.V. Ammosov, N.B. Delone, and V.P. Krainov, Zh. Éksp. Teor. Fiz. **91**, 2008 1986) [Sov. Phys. JETP **64**, 1191 (1986)].
[9] V.P. Krainov, J. Opt. Soc. Am. B **14**, 425 (1997).
[10] B. Walker, B. Sheehy, L.F. Di Mauro, P. Agostini, K.J. Schafer, and K.C. Kulander, Phys. Rev. Lett. **73**, 1227 (1994) and references therein.
[11] S.F.J. Larochelle, A. Talebpour, and S.L. Chin, J. Phys. B **31**, 1215 (1998).
[12] D.N. Fittinghoff, P.R. Bolton, B. Chang, and K.C. Kulander, Phys. Rev. Lett. **69**, 2642 (1992).
[13] S.F.J. Larochelle, A. Talebpour, and S.L. Chin, J. Phys. B **31**, 1201 (1998).
[14] A. Becker and F.H.M. Faisal, Phys. Rev. A **59**, R1742 (1999).
[15] D. Dundas, K.T. Taylor, J.S. Parker, and E.S. Smyth, J. Phys. B **32**, L231 (1999).
[16] P.B. Corkum, Phys. Rev. Lett. **71**, 1994 (1993).
[17] G.N. Gibson, G. Dunne, and K.J. Bergquist, Phys. Rev. Lett. **81**, 2663 (1998).
[18] A. Talebpour, S.F.J. Larochelle, and S.L. Chin, J. Phys. B **31**, L49 (1998).
[19] A. Talebpour, S.F.J. Larochelle, and S.L. Chin, J. Phys. B **31**, 2769 (1998).
[20] M.J. DeWitt and R.J. Lewis, J. Chem. Phys. **108**, 7045 (1998).
[21] A.I. Pegarkov, E. Charron, and A. Suzor-Weiner, J. Phys. B **32**, L363 (1999) and private communication.
[22] L.J. Frasinski, K. Codling, and P. Hatherly, Phys. Lett. A **142**, 499 (1989).
[23] P. Maine, D. Strickland, P. Bado, M. Pessot, and G. Mourou, IEEE J. Quantum Electron. **QE−24**, 398 (1988).
[24] A. Laubereau, *Ultra−short Laser Pulses: Generation and Applications*, edited by W. Kaiser (Springer, Berlin, 1993), pp. 35−112.
[25] S. Bollanti, P. Di Lazarro, and D. Murra, Opt. Commun. **134**, 503 (1997).
[26] A. Yariv, *Quantum Electronics* (Wiley, New York, 1989).
[27] Ph. Hering and C. Cornaggia, Phys. Rev. A **59**, 2836 (1999).
[28] A.M. Perelomov and V.S. Popov, Zh. Éksp. Teor. Fiz. **52**, 514 (1967) [Sov. Phys. JETP **25**, 336 (1967)].
[29] C.H. Greene, A.R.P. Rau, and U. Fano, Phys. Rev. A **26**, 2441 (1982).
[30] Y. Liang, A. Talebpour, C.Y. Chien, S. Augst, and S.L. Chin, J. Phys. B **30**, 1369 (1997).
[31] C. Guo, M. Li, J.P. Nibarger, and G.N. Gibson, Phys. Rev. A **58**, R4271 (1998).
[32] T. Auguste, P. Monot, L.A. Lompré, G. Mainfray, and C. Manus, J. Phys. B **25**, 4181 (1992).